SARS-CoV-2 variants of concern exhibit differential gastro-intestinal tropism and pathogenesis in the Syrian golden hamster model.

Authors: Santhosh K. Nagaraj*[1,2], Christy M. Joy*[1,2], Rohan Narayan[1,2], Rishad Shiraz[1,2], Sumandeep Kaur[1,2], Oyahida Khatun[1,2], Sagar Dubey[1,2], Shashank Tripathi[1,2]

Correspondence: shashankt@iisc.ac.in

Affiliation:

[1]Emerging Viral Pathogens Laboratory, Infosys Wing, Centre for Infectious Disease Research, Indian Institute of Science; Bengaluru, 560012, India.

[2]Department of Microbiology and Cell Biology, Division of Biological Sciences, Indian Institute of Science; Bengaluru, 560012, India.

Abstract

The Coronavirus Disease 2019 (COVID-19) pandemic caused by Severe Acute Respiratory Syndrome Coronavirus 2 (SARS-CoV-2) has taken its toll on worldwide public health infrastructure. SARS-CoV-2 is reported to exhibit wide tissue tropism, contributing to its severe pathogenicity that often culminates in multiple-organ failure. The onslaught of this disease has intensified due to the emergence of variants of concern (VOC), such as Delta and Omicron. These variants have been linked to gastrointestinal (GI) symptoms, suggesting a potential fecal-oral route of viral transmission. Here we compared the broad tissue tropism of ancestral Hong-Kong SARS-CoV-2 (SARS-CoV-2 HK) against Delta and Omicron VOCs in aa hamster model by analyzing tissue samples collected from the upper and lower respiratory system and the GI tract. We observed an overall increase in vRNA load and pro-inflammatory cytokines, especially in GI tracts of animals infected with Delta virus, indicating selective virus tropism and pathology in these tissues. However, no apparent spike in Delta viral load was observed in the large intestine and fecal matter. Overall, our research investigates the wide range of tissues that various SARS-CoV-2 strains can infect in hamsters and presents evidence supporting the increased preference of Delta VOCs for infecting the GI tract.

Keywords: SARS-CoV-2, GI infection, hamster, VOCs, tissue tropism, feces

Introduction

Coronavirus Disease-19 (COVID-19) is a respiratory infection caused by Severe Acute Respiratory Syndrome Virus-2 (SARS-CoV-2), which is enveloped by positive-sense single-stranded RNA viruses of genus Betacoronavirus, family Coronaviridae (1). The virions are decorated with surface glycoproteins called Spike, which give the appearance of a crown (2). The SARS-CoV-2 spike glycoprotein binds to angiotensin-converting enzyme 2 (ACE2) receptors, and entry into permissive cells is facilitated by cleavage of spike by host proteases like transmembrane protease serine 2 (TMPRSS2) at the cell surface and cathepsin L in endosomes (3) (4).

The virus was first detected in patients epidemiologically linked to the Huanan wet market in Wuhan, China in December 2019 (5, 6). Since then, SARS-CoV-2 has spread throughout the globe, causing ~7 million deaths worldwide as of May 2023 (https://covid19.who.int/). The inherent airborne transmission capability of SARS-CoV-2 and high mutation rates associated with genome plasticity has favored high rates of human-human transmission of the virus on a global scale (7). This has also led to the emergence and spread of novel variants of concern (VOC) which have acquired heightened immune escape, transmission, and fitness advantages. These VOCs, designated Alpha, Beta, Delta, and Omicron variants have emerged independent from one another and throughout the pandemic, become dominant regionally or globally, outperforming previous variants (8). The large-scale use of effective vaccines and antivirals has brought the virus under control, but positive cases still occur sporadically (9).

SevereSevere SARS-CoV-2 infection often results in extrapulmonary manifestations that include gastrointestinal, cardiovascular, hematologic, renal, neurologic, ophthalmologic, and dermatologic systems (10, 11). The governing factors for such broad cell tropism of SARS-CoV-2 mainly include ACE2 distribution across tissues (11) and comorbidities or immunocompromised status of individuals who are more prone to severe infection (12). The pathogenicity of a virus can vary depending on multiple factors, including the host species, immune response, and other genetic and environmental factors. Studies involving animal models, such as hamsters, are valuable for understanding viral pathogenesis and assessing the effectiveness of

potential therapeutics or vaccines against COVID-19 (13). HereHere we compared the tissue tropism of the most clinically relevant strains of SARS-CoV-2 in the golden hamster model, which is a highly susceptible model that phenocopies several clinical aspects of COVID-19 (14, 15). We compared infection and tissue tropism of parental SARS-COV-2 HK strain with Delta and Omicron VOCs in hamsters and found the Delta virus to be more prone to infect the GI tract and possibly contribute to fecal transmission.

MATERIAL AND METHODS

Virus stocks

SARS-CoV-2 Isolate Wuhan (hCov-19/Hong Kong/VM20001061/2020, Cat No.: NR-52282), Delta variant (USA/PHC658/2021, Lineage B.1.617.2; Cat No.: NR-55611,) and Omicron variant (USA/PHC658/2021, Cat No.: NR-56461) were obtained from BEI Resources, NIAID, NIH. All viruses were propagated and titrated by plaque assay in VEROERO-E6 cells as previously described (16).

Ethics statement

This study was conducted in compliance with institutional biosafety guidelines, (IBSC/IISc/ST/17/2020; IBSC/IISc/ST/18/2021), following the Indian Council of Medical Research and Department of Biotechnology recommendations. All experiments involving animals were reviewed and approved by the Institutional Animal Ethics Committee (Ref: IAEC/IISc/ST/784/2020) at the Indian Institute of Science. The experiments were performed according to CPCSEA (The Committee for Control and Supervision of Experiments on Animals) guidelines.

Animals

Male and Female Syrian Golden Hamsters (*Mesocricetus auratus*) of 6-7 weeks old (60-70 g) were obtained from Biogen Laboratory Animal Facility, Bengaluru, India. All the animal experiments were conducted in the viral Biosafety level-3 Laboratory at, the Indian Institute of Science, Bangalore. Animals (n=3) were maintained in individually ventilated cages at 23±1°C temperature and 50±10% relative humidity with 12 h day/night light cycle with food and water *ab libitum*. An overdose of

Ketamine (Bharat Parenterals Limited) and Xylazine (Indian Immunologicals Ltd) was used to sacrifice animals upon completion of the experiment.

Grouping and virus infection

A total of 28 animals were divided into 7 different groups with 2 males and 2 females per group. The animals from respective groups were intraperitoneally anesthetized (Ketamine-150mg/kg; Bharat Parenterals Limited and Xylazine-10mg/kg; Indian Immunologicals Ltd.) and infected intranasally with either Hongkong, Delta, or Omicron virus at the dose of 10^5 and 10^6 Plaque Forming Units (PFU)/animal in 100 µL PBS (50µL/nostril). Fresh Feces (in Trizol) and Nasal washes were collected (in 100 µL PBS) before infection, on 2 and 4 days post-infection (Fig.1B). All animals were sacrificed on day-4 post-infection, and blood was collected by cardiac puncture. Sera were separated and stored at -80ºC until further use. Organs such as lungs, esophagus, stomach, small intestine, and large intestine were stored in Trizol (for RT-PCR) or DMEM (for plaque assay). A part of each organ was used to estimate the viral RNA load by RT-PCR or plaque assay and another portion for histopathological analysis.

Clinical signs

After infection, hamsters were daily observed for the following clinical signs till day 4 p.i. and scored based on severity; Lethargy (none=0, mild=1, moderate=2, severe=3); piloerection (none=0, mild=1, moderate=2, severe=3); abdominal respiration (absent=0, present=1); hunched back (absent=0, present=1) and body weight loss (1-5 %= 1; 6-10%=2; 11-15%=3).

Scoring of lung gross pathology

The lungs were scored for focal and diffused hyperemia. Based on the severity of hyperemia, scoring was given on a scale of 1 to 3 (mild=1, moderate=2, severe=3). The total lung weight was recorded and images were captured. The lung-body weight ratio was calculated for each animal on the day of dissection.

Lung viral plaque assay

The plaque assay was performed to determine the viral titer for the tissue homogenates on VERO-E6 cells in 12-well plates. Briefly, plates were seeded with 0.2 x 10^6 cells/mL and incubated for 48h at 37ºC. All the samples were serially diluted 10-fold in DMEM with 2 % FBS. A 100 µL of the diluted sample was added to each well in duplicates and incubated at 37ºC for 1 h with shaking every 10-15 min. After incubation, the inoculum was removed completely, overlayed with 1 mL of 0.6 % Avicel and kept at 37ºC with 5 % CO2 for 48 h. The overlay was removed completely post-incubation and cells were fixed by adding 1 mL/well of 4% formaldehyde in PBS. Cells were stained with 1% crystal violet solution to visualize the plaques.

RNA extraction and viral load by Quantitative Real-Time PCR (qRT-PCR)

All the organs were processed using a FastPrep-24™ stainless-steel bead homogenizer (MP Biomedicals, USA) and total RNA was extracted using TRIzol (15596018, Thermo Fisher) as per the manufacturer's instructions. RNA from fecal matter was extracted using the QiaAMP viral RNA mini kit (Cat No. 52906, Qiagen, US) according to the manufacturer's instructions. A 10µL reaction mixture with 100ng of RNA per sample, in a 384-well block was used to quantify viral RNA using AgPath-ID™ One-Step RT-PCR kit (AM1005, Applied Biosystems). The following primers and probes targeting the SARS CoV-2 N-1 gene were used. Forward primer: 5'GACCCCAAAATCAGCGAAAT3' and Reverse primer: 5' TCTGGTTACTGCCAGTTGAATCTG3', Probe: (6-FAM/BHQ-1) ACCCCGCATTACGTTTGGTGGACC. The Ct values were used to determine viral copy numbers by generating a standard curve using SARS CoV-2 genomic RNA standard.

Cytokine gene expression by qRT-PCR

The host mRNA expression of IFN-γ, IL-6, and TNF-α was quantified using suitable primers with 18s RNA as an internal reference gene. Briefly, cDNA was prepared from 1µg RNA using PrimeScript^{TM} RT reagent Kit with gDNA Eraser (TaKaRa). RT-qPCR was performed using 2.5 µL of cDNA, 2.5 µL of the primer mix, and 5 µL of SYBR™ Green PCR Master Mix (Applied Biosystems). The following primers for hamster IFN-γ, IL-6, and TNF-α genes were used. **IFN-γ:** Forward primer: 5'TGTTGCTCTCTCTCTCTCAGG3' and Reverse primer:

5'AAGACGAGGTCCCCTCCATTC3'. **IL-6:** Forward primer: 5'AGGCCATCCTGATGGAGAAG3' and Reverse primer: 5' GGTATGCTAAGGCACAGCAC3'. **TNF-α:** Forward primer: 5'TGAGCCATCGTGCCAATG3' and Reverse primer: 5'AGCCCGTCTGCTGGTATC3'. The comparative threshold (Ct) values were used to calculate the mean Log_2 fold change compared to 18S RNA by the delta-delta Ct method.

Cytokine ELISA

The sera obtained from hamsters on day 4 p.i. were used to evaluate the level of IFN-□ and IL-4 cytokines by sandwich ELISA method using a commercially available kit (ImmunoTag™, USA). The sensitivity of both IFN-□ and IL-4 kit was 9.375 pg/mL.

Histopathology and Immunohistochemistry

Tissue specimens were fixed in 4% paraformaldehyde in PBS and embedded in paraffin blocks. Tissue sections of 4-6 µm thickness were stained with Hematoxylin and Eosin (H&E). Slides were examined by light microscopy for 3 histological criteria in the lung (Alveolar infiltration and exudation, vasculature inflammation, and peribronchiolar infiltration with epithelial desquamation). Based on the severity, each criterion was scored on a scale of 1 to 3.

The protocol for Immunohistochemistry (IHC) was modified from a previous report (17). Briefly, IHC of the duodenum samples was performed on 5µm paraffin-embedded tissue sections placed on the poly L-lysine coated slides. The sections were deparaffinized and hydrated using xylene and descending grades of alcohol respectively. Antigen retrieval was carried out by heating in sodium citrate buffer (10 mM, pH 6.0) for 15 minutes using a domestic pressure cooker in a steam setting. The sections were quenched for endogenous peroxidase using 3% hydrogen peroxide and protein blocked using 3% Bovine Serum Albumin (BSA) for 20 min each at RT. Slides were then incubated with a primary antibody for SARS-CoV-2 nucleocapsid protein (Novus Biological, NB 100-56576) at 4 °C overnight. Detection was performed using a goat anti-rabbit HRP secondary antibody (Invitrogen, 31460) for 60 min at RT and visualized using 3,3-diaminobenzidine (DAB) (Sigma,

11718096001) for 10 min at RT. Counterstaining was done with Harry's Haematoxylin for 1 min. After dehydration and air drying, the sections were cleared in xylene and mounted using Dibutylphthalate polystyrene xylene (DPX) mountant. The mounted slides were viewed under the microscope and representative images were recorded.

Statistical analysis

The data were analyzed using GraphPad Prism v 8.4.3 and represented as mean ±SEM. Statistical variations were determined by one-way ANOVA (Lung/bodyweight ratio, tissue viral RNA load, and cytokine mRNA level) or two-way ANOVA (Body weight, clinical signs) with Dunnett's multiple comparisons tests or by paired T-test (Lung histopathology). Values were significant when $*P < 0.05$, $**P < 0.01$ or $***P < 0.001$.

Results

Comparison of clinical signs and lung viral load in Syrian Hamsters infected with Delta, Omicron VOCs and ancestral SARS-CoV-2 strain.

Here, we compared the pathogenicity of SARS-CoV-2 HK against Delta (lineage B.1.617.2) and Omicron (lineage B.1.1.529) VOCs. SARS-CoV-2 HK was originally isolated from a nasopharyngeal aspirate and throat swab collected from an adult male patient on January 22, 2020, in Hong Kong, China. The strain is assigned to lineage A and has been used as part of vaccine preparations (https://www.beiresources.org/Catalog/animalviruses/NR-52282.aspxhttps://www.beiresources.org/Catalog/animalviruses/NR-52282.aspx) (16). The Delta variant emerged in India in late 2020 and the Omicron in Botswana in November 2021 (18, 19). Delta variant was associated with higher pathogenicity compared to ancestral or other strains causing more severe illness and hospitalization rates (18). On the other hand, the Omicron variant was phylogenetically distinct and possessed over 30 mutations in the spike protein (9, 20). Nucleotide mapping comparing these three viruses is shown in **(Fig. 1A).**

To understand the pathogenicity and tissue tropism of SARS-CoV-2 HKHK in comparison with Delta and Omicron strains, the body weight, clinical signs, and viral replication in lungs and gastrointestinal tract were assessed post-infection at two

different doses of 10^5 and 10^6 PFU in hamsters. The viral shedding was also assessed in the nasal route or fecal matter collected at days 0, 2, and 4 post-infections **(Fig. 1B).** The body weight was reduced until 4 days post-infection (dpi) among all the three strains used. The Delta-infected hamsters had more drop in body weight and Omicron infection caused the least reduction in body weight in comparison with control-uninfected animals **(Fig. 1C).** The clinical signs in virus-infected hamsters also showed a similar pattern as of body weight among the strains used. Only Omicron-infected hamsters remained subclinical and started recovering from the drop in body weight **(Fig. 1D).** The viral RNA load as examined by RT-PCR was higher in both SARS HK and Delta-infected hamsters when compared to Omicron. The infectious viral titer as observed by plaque assay also showed a similar pattern of viral load **(Fig. 1F).** The nasal wash samples collected on day 2 showed that Omicron infection resulted in a similar viral load as Delta and Hongkong strain. However, on 4 dpi, the viral burden was lesser in the nasal region of Omicron-infected hamsters **(Sup Fig 1 A, B).**

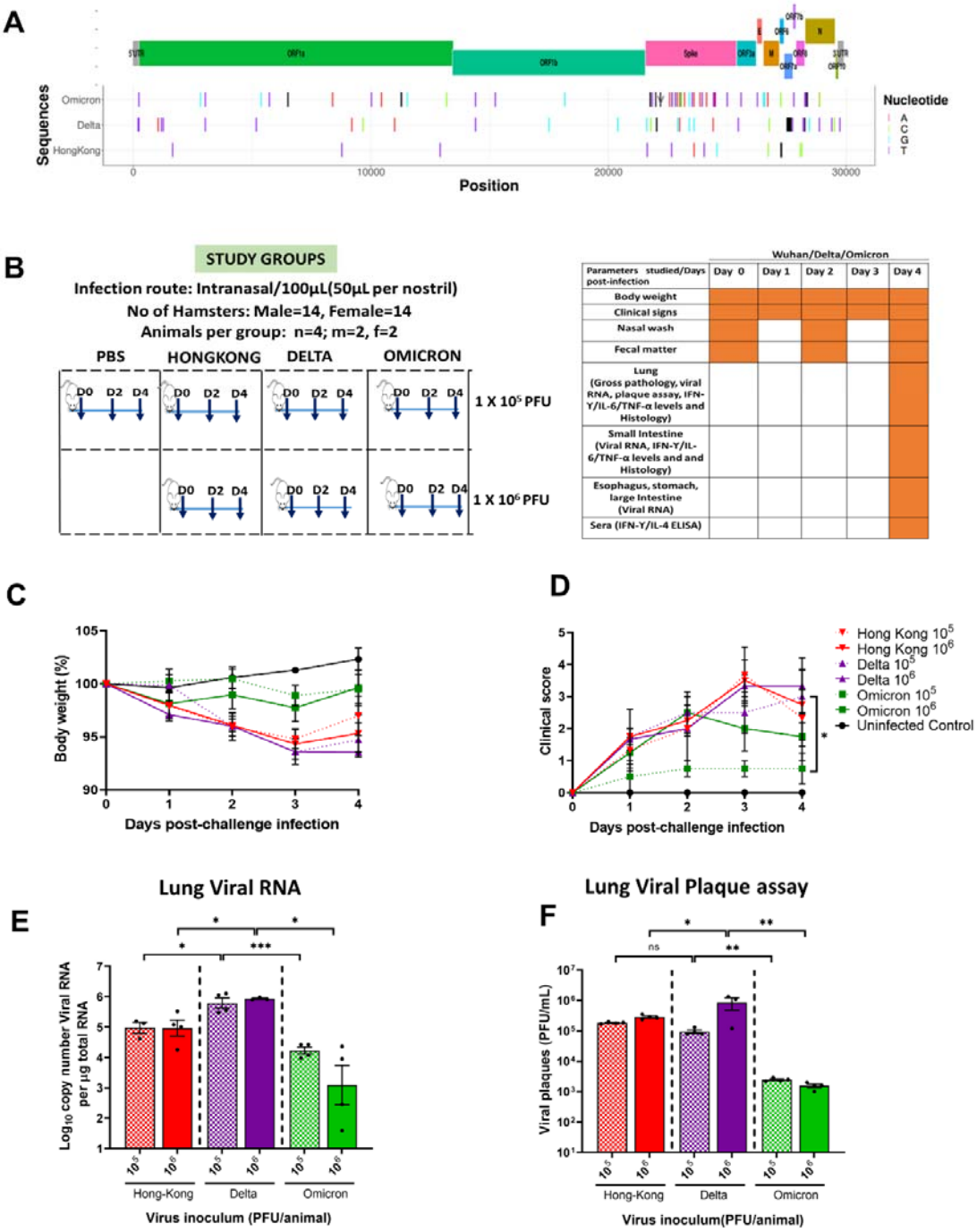

Figure1. (A) SARS-CoV-2 nucleotide mutation mapping of Hongkong, Delta, and Omicron compared to the Wuhan reference sequence. X-axis represents nucleotide position in the genome and Y-axis shows the different sequence isolates used. Single nucleotide polymorphisms and deleted nucleotide positions are marked using "|", with black indicating a nucleotide deletion and different colors denoting different nucleotide substitutions. Insertions are marked using "v" in dark grey color. The 5'

and 3' untranslated Regions are marked in grey and the different ORFs and structural proteins are represented in different colors. **(B)** Outline of the work plan followed in this study. **(C)** Percentage bodyweight of hamsters (n=3 to 4) monitored over 4 dpi, normalized to mean weight measured at Day 0. **(D)** Clinical signs in hamsters (n=3 to 4) including piloerection, abdominal respiration, hunched back, and lethargy were monitored over 4 dpi and scored from 1-4 based on severity. **(E)** The total SARS CoV-2 viral RNA copy number in the lung was estimated by qRT PCR. **(F)** Infectious SARS-CoV-2 titer was quantified by plaque assay. For statistics, data corresponding to the two doses of Delta were compared respectively against Hong Kong and Omicron viruses. * $p<0.05$ by paired t-test. Error bars indicate Mean ± SEM.

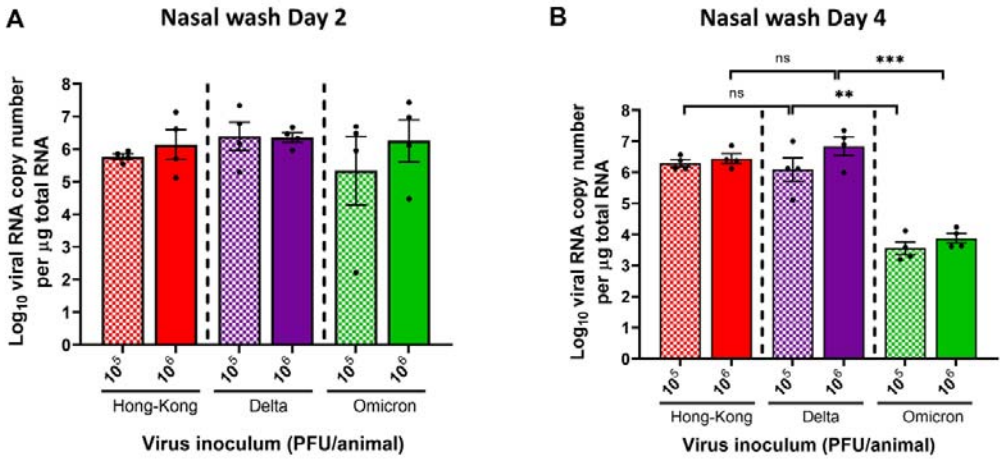

Supplementary Figure 1. (A-B) Hamsters were infected with either 10^5 or 10^6 PFU/animal of SARS-CoV-2 Hong-kong strain, or VOCs Delta or Omicron. Nasal washes were collected from animals at **(A)** 2 and **(B)** 4 dpi and viral RNA was estimated by qRT PCR.

Comparison of lung pathology and inflammatory cytokine expression in Syrian Hamsters infected with Delta, Omicron VOCs and Ancestral SARS-CoV-2 strain.

The hamsters infected with Delta showed more gross pathological changes than SARS-CoV-2 HK and HK Omicron variants at 4 dpi. which was consistent with the viral load data obtained from RT-PCR and plaque assay. Further, at 10^5 PFU dose,

Omicron infected hamsters didn't show any visible pathology **(Fig. 2A and 2B).** Additionally, the lung-bodyweight ratio was higher in Delta-infected hamsters with Hongkong and Omicron-infected hamsters having a lesser but similar lung-body weight ratio (**Fig. S2**). The hamsters infected with Delta had relatively higher levels of lung inflammatory cytokines such as TNF-α **(Fig. 2C)**, IFN-□ **(Fig. 2D),** and IL-6 **(Fig. 2E)** than Hongkong and Omicron variants at both doses studied. It's interesting to note that, Omicron infection led to a similar level of cytokines expression when compared to Hongkong infected hamsters. Further, IL-6 levels were consistently lower among all the strains studied at 10^6 PFU in comparison with 10^5 PFU as inoculum.

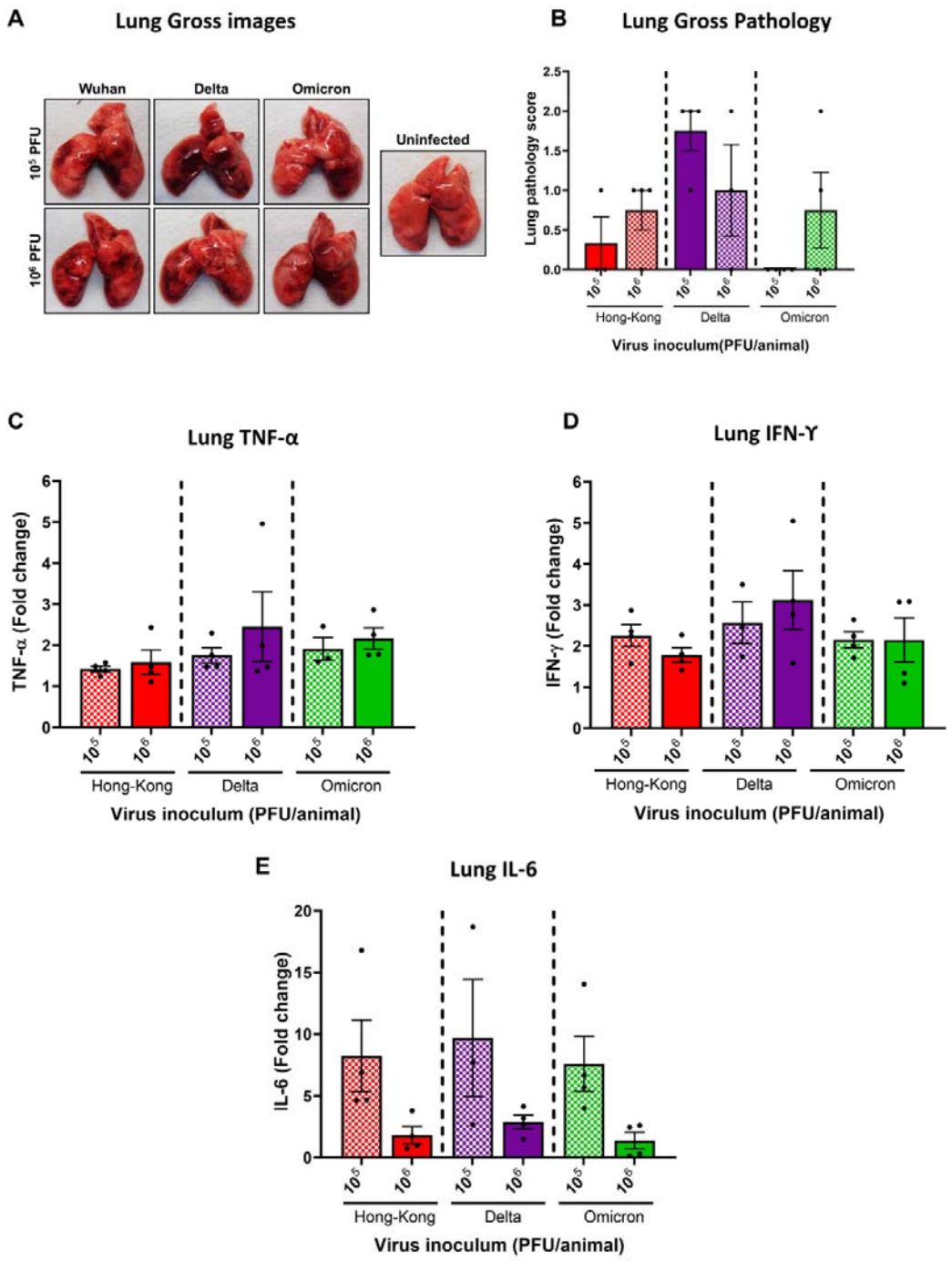

Figure 2. (A-E) Hamsters were infected with either 10^5 or 10^6 PFU/animal of SARS-CoV-2 Hong-kong strain, or VOCs Delta or Omicron. **(A)** Hamsters were sacrificed at 4 dpi and images of whole lungs were captured. **(B)** Lung gross pathology was scored 1-3 based on the increasing severity of focal or diffused hyperemia. Animals were sacrificed 4 dpi and a portion of the lungs was stored In TriZol. Total RNA was

extracted and used to quantify expression levels of **(C)** TNF-α, **(D)** IFN-□, and **(E)** IL-6 by qRT PCR.

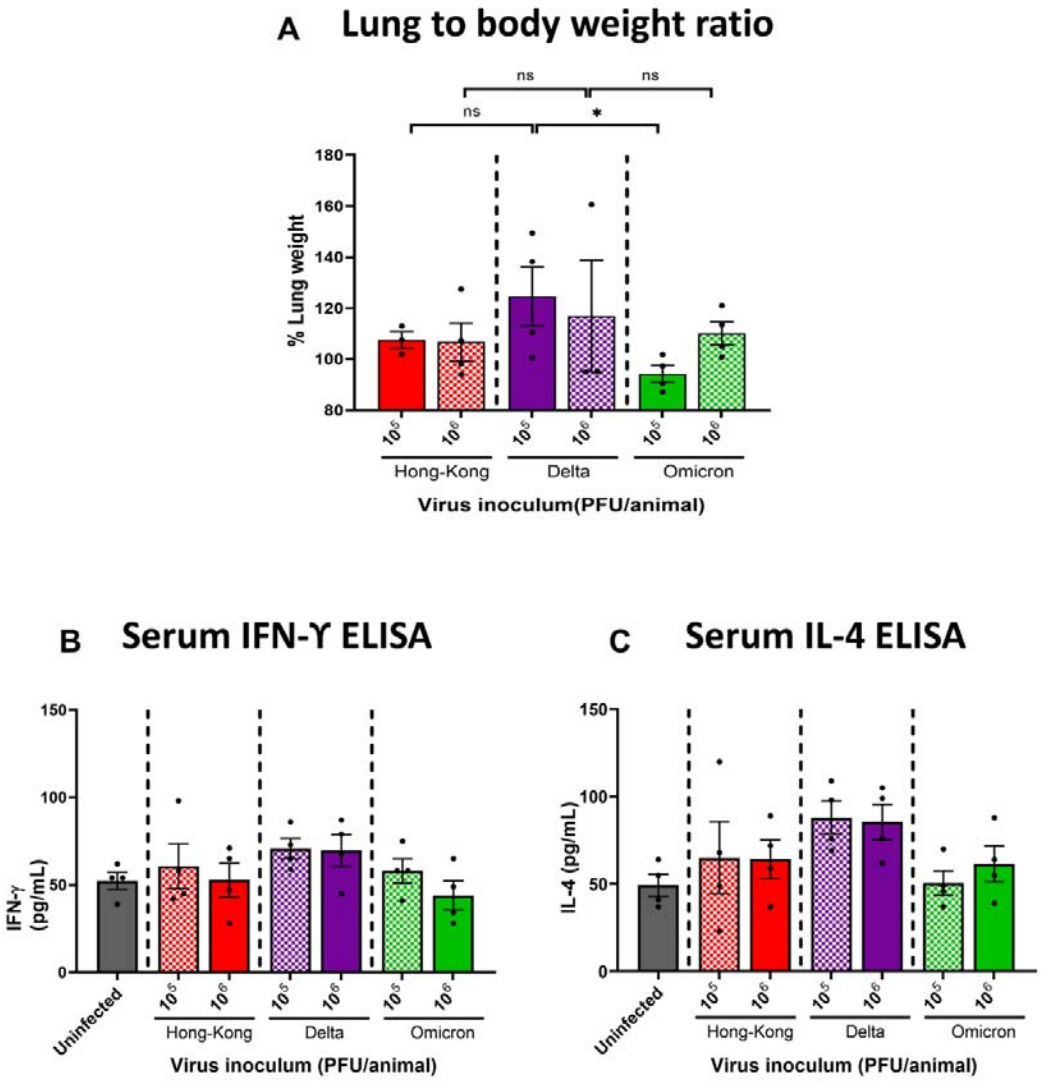

Supplementary Figure 2. (A-C) Hamsters were infected with either 10^5 or 10^6 PFU/animal of SARS-CoV-2 Hong-kong strain, or VOCs Delta or Omicron. **(A)** The total weight of the lungs was used to plot the lung-body weight ratio. Animals were sacrificed 4 dpi and serum was collected from hamsters and used to quantify **(B)** IFN-gamma and **(C)** IL-4 using a commercially available ELISA kit.

Comparison of lung histopathology and viral antigen localization in Syrian Hamsters infected with Delta, Omicron VOCs and Ancestral SARS-CoV-2 strain.

The histopathological assessment of SARS-CoV-2 infected hamster lungs collected on 4 dpi revealed bronchointerstitial pneumonia including vascular inflammation, alveolar infiltration, and Peribronchiolar infiltration with necrosis. Mononuclear cell infiltrations were also observed in peribronchial and perivascular areas with occasional neutrophils. These lesions, mainly vascular inflammation were more severe in Delta-infected hamsters, especially at 10^6 PFU dose **(Fig. 3A).** The cumulative histopathological lung scores were highest in Delta-infected hamsters, with significant difference between SARS-CoV-2 HK and Delta-infected groups. Consistent with other data, Omicron-infected hamsters showed lung pathological changes similar to as observed in Hongkong infected hamsters **(Fig. 3B).**

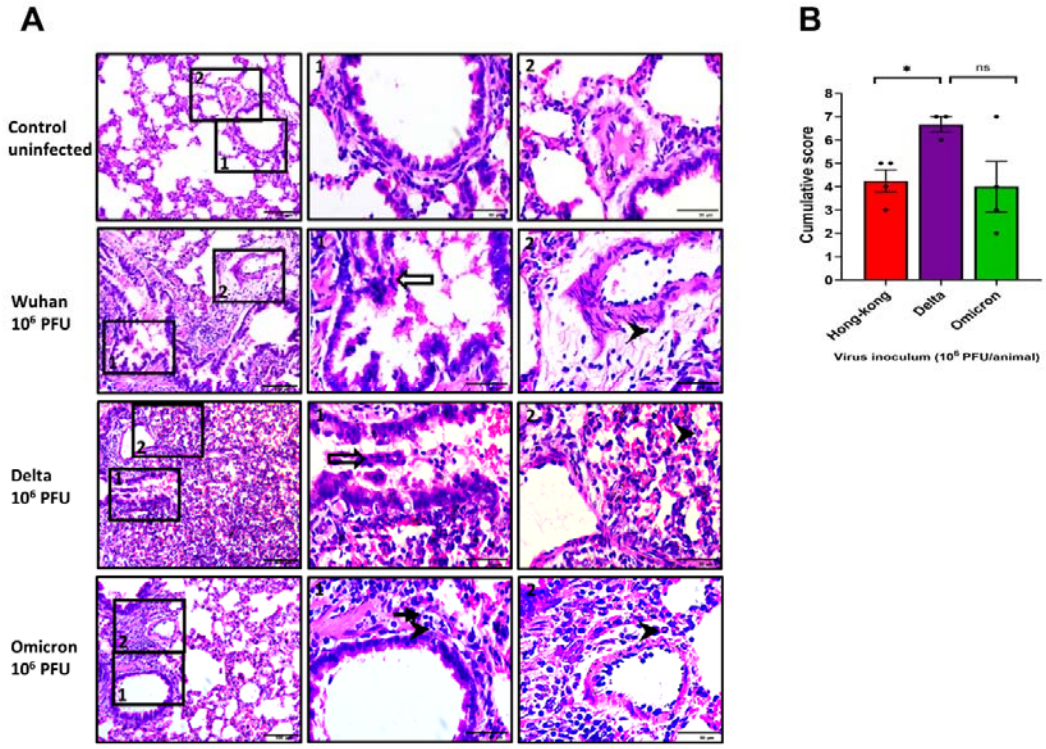

Figure 3 (A-B). (A) Histopathology sections of 10^6 PFU/animal group showed (1) bronchial epithelial necrosis and inflammatory changes (2) vascular inflammation (3)

alveolar wall thickening and inflammatory cell infiltration. Bronchial and vascular changes are represented in insets 1 and 2 respectively (200x magnification), while alveolar thickening is in the first column of the figure set (100x magnification). White arrows indicate denuded necrotized bronchiolar epithelial cells admixed with inflammatory cells in the airway lumen, whereas inflammatory cell infiltration in peribronchiolar and perivascular areas are indicated as black arrows (lymphocytes) and black arrowheads (neutrophils). **(B)** Cumulative histopathology scoring was plotted for each group with the selected criteria.

Comparison of viral RNA load and inflammatory marker expression in the GI tract of Syrian Hamsters infected with Delta, Omicron VOCs and Ancestral SARS-CoV-2 strain.

At both the 10^5 and 10^6 PFU doses tested, the viral RNA load was consistently higher in the esophagus, stomach, and small and large intestines of Hongkong and Delta-infected hamsters, with lower viral RNA load being detected in these tissues of Omicron-infected hamsters **(Fig. 4A-D).** Interestingly, the viral RNA load in the small intestine was highest in the Delta-infected hamsters (5.24 log) when compared to Hongkong or Omicron-infected hamsters. Also, viral RNA copy numbers were similar in the large intestine among the Hongkong and Delta-infected hamsters. Surprisingly, the fecal matter collected on 2 and 4 dpi showed a relatively higher viral RNA load in Hongkong-infected hamsters rather than in Delta-infected hamsters **(Fig. S3).**

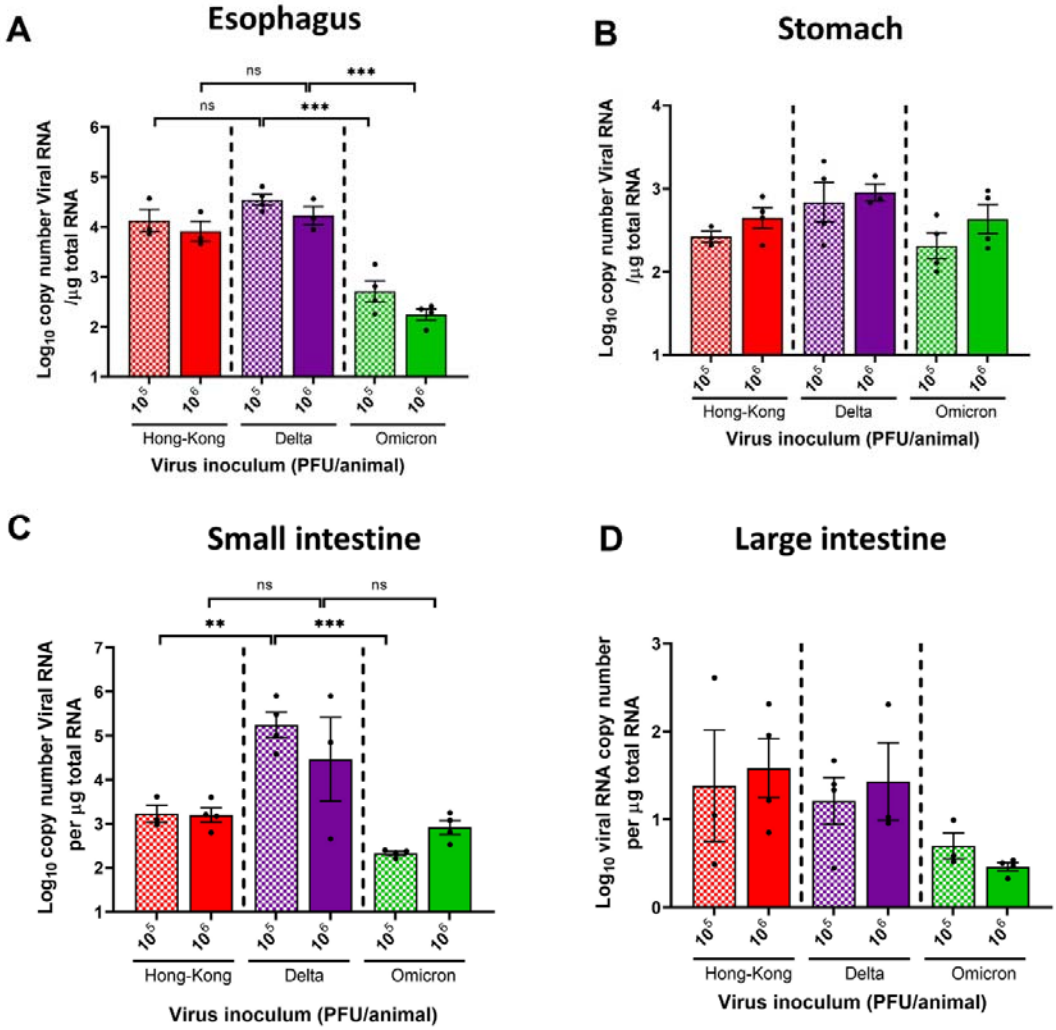

Figure 4 (A-D). Hamsters were infected with 10^5 and 10^6 PFU/animal of SARS-CoV-2 Hong-Kong strain, or VOCs Delta or Omicron. Animals were sacrificed at 4 dpi and a portion of **(A)** esophagus, **(B)** stomach, **(C)** small, and **(D)** large intestines were stored In TriZol. Total RNA was extracted and viral RNA copy number was quantified by qRT-PCR.

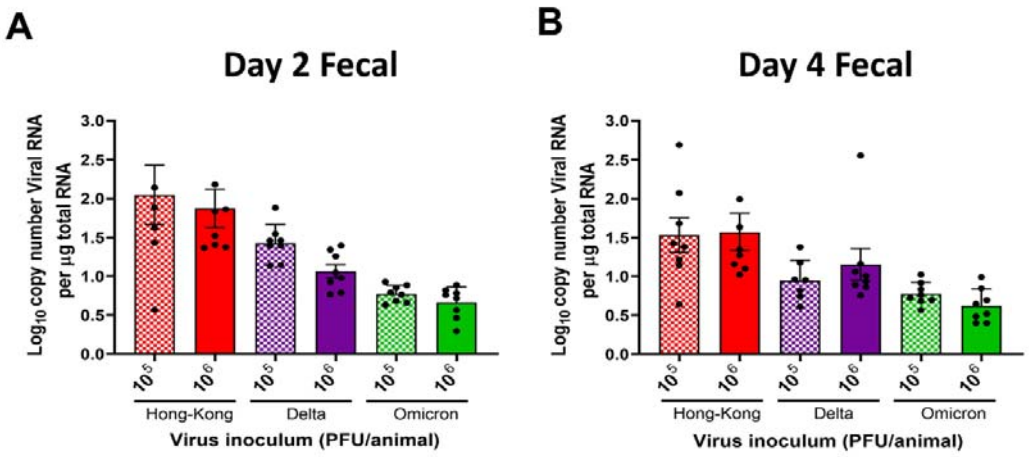

Supplementary Figure 3. (A-B) Hamsters were infected with either 10^5 or 10^6 PFU/animal of SARS-CoV-2 Hong-kong strain, or VOCs Delta or Omicron. The fecal matter was collected freshly from each animal group at **(A)** 2 and **(B)** 4 dpi and the viral RNA copy number was estimated by qRT PCR.

Delta VOC of SARS-CoV-2 infects and causes pathology in the small intestine of Syrian hamsters.

To understand the SARS-CoV-2 strain-induced pathology in the regions of the small intestine, their epithelial morphometric analysis was performed. Here, the villus length and Cyrpt depth were measured and their ratio was determined. The small intestines harvested from hamsters infected with Delta variant at both 10^5 and 10^6 PFU doses had higher crypt depth and lesser villi length to crypt depth ratio than Hongkong or Omicron-infected hamsters which were also statistically significant compared to the uninfected control hamsters **(Fig. 5A-D).** The Villous length of all groups was comparable and didn't show any significant difference. In Hongkong and Omicron-infected hamsters, even though they had relatively similar villi length to crypt depth ratio, Omicron-infected hamsters had higher epithelial crypt depth **(Fig. 5B-D).).**

The immunohistochemical staining also showed the higher presence of SARS-CoV-2 nucleocapsid protein in the duodenum epithelial cells of the small intestine harvested from Delta-infected hamsters **(Fig 5E).** Overall, these data emphasize the small intestine mucosal damage and subsequent regenerative changes possibly caused by the Delta strain. Further correlating with these data, cytokine levels such as IFN-□,

TNF-α, and IL-6 were relatively higher in the small intestines harvested from Delta-infected hamsters with similar levels observed among the Hongkong and Omicron-infected hamsters **(Sup Fig. 4 A-C).** Notably, IFN-□ level was very high (≈ 3 fold) during Delta infection when 10^5 PFU was used as inoculum **(Sup Fig. 4 A).).**

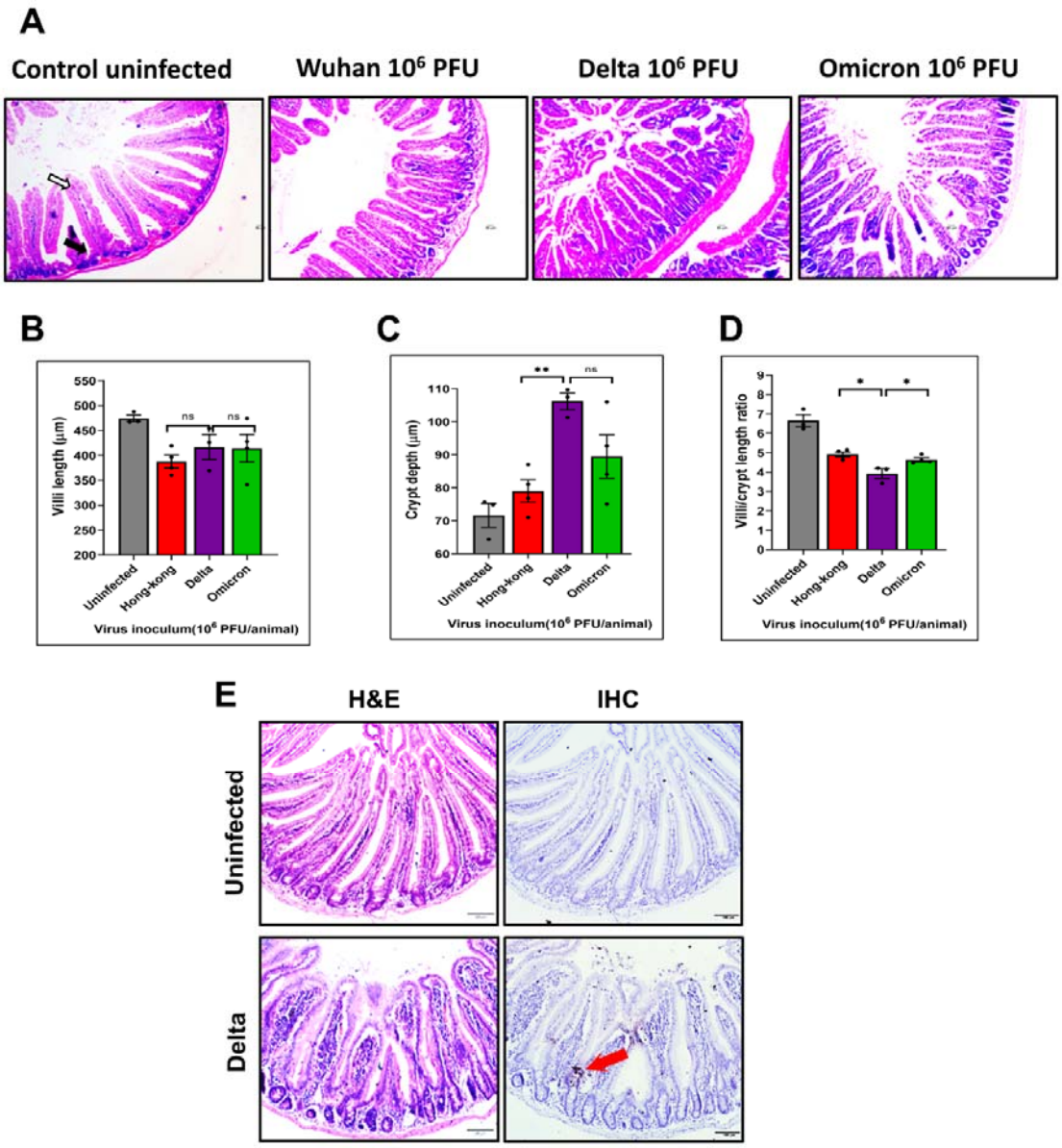

Figure 5. (A-E) Hamsters were infected with 10^6 PFU/animal of SARS-CoV-2 Hong-Kong strain, or VOCs Delta or Omicron. Animals were sacrificed at 4 dpi and small intestine was collected and processed for histology. **(A)** Representative H & E stained sections of duodenum of normal and different infected groups at 40x

magnification. The black arrow shows the crypt and the white arrow indicates villi. **(B-D)** Villi and crypt length were quantified using ImageJ/Fiji. Data shown indicate **(B)** Villi length, **(C)** Crypt length, and **(D)** ratio of villi to crypt length. Data from 8-10 villi-crypt units per animal were measured (n=3-4 per group). **(E)** H&E staining of the duodenum of uninfected and SARS CoV-2 delta VOC challenged hamsters (left) and Immunohistochemistry analysis (right) with the red arrow indicating the presence of SARS-CoV-2 N protein. Statistical measurements were done by comparing Delta to Hong Kong and Omicron. * $p<0.05$, ** $p<0.01$ by paired t test. Error bars indicate mean ±SEM.

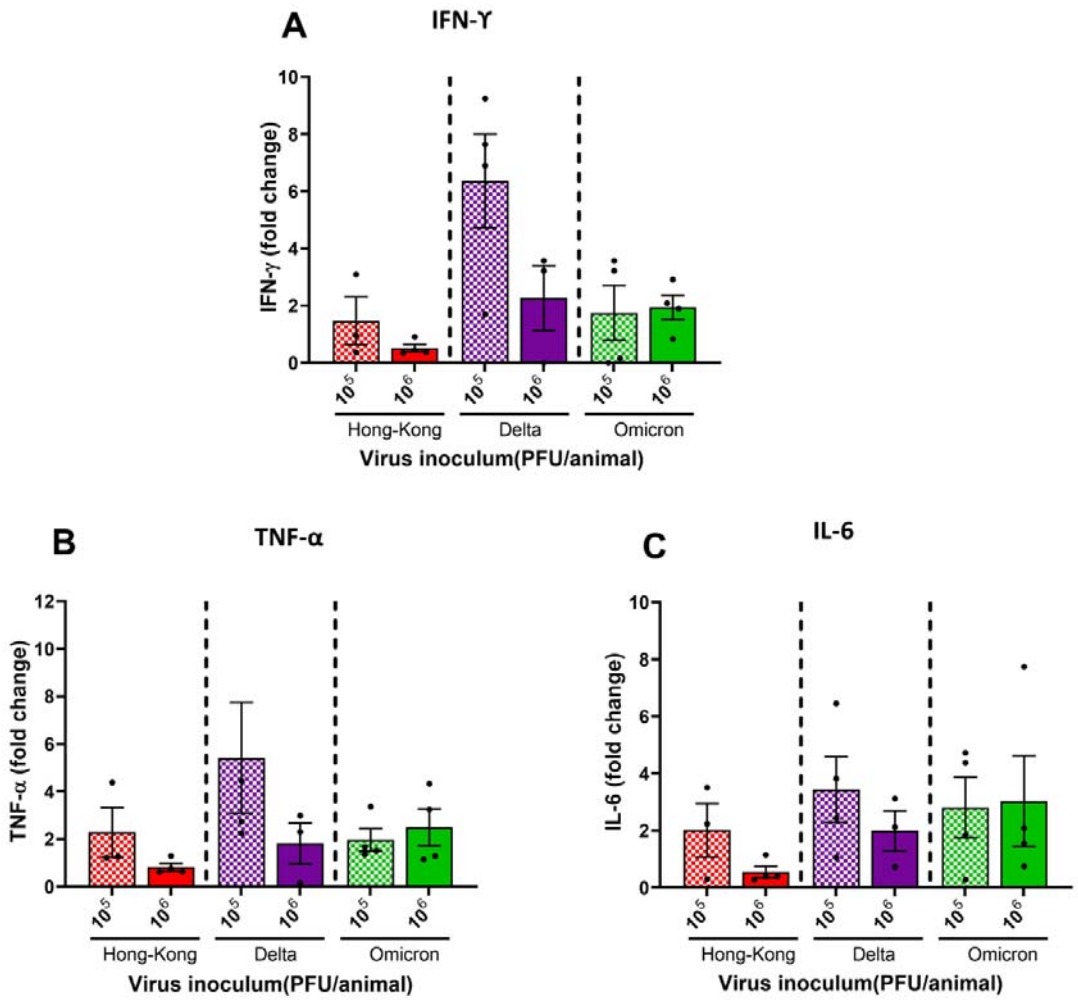

Supplementary Figure 4. (A-C) Hamsters were infected with either 10^5 or 10^6 PFU/animal of SARS-CoV-2 Hong-kong strain, or VOCs Delta or Omicron. Animals were sacrificed at 4 dpi and a portion of small intestines was stored In TriZol. Total

RNA was extracted and used to quantify expression levels of **(A)** IFN-□, **(B)** TNF-α, and **(C)** IL-6 by qRT PCR.

Discussion

In this study, the SARS-CoV-2 ancestral strain (HK) and Delta VOC infection in hamsters displayed enhanced clinical signs and higher viral load in the upper respiratory tract, while the Omicron variant caused attenuated clinical signs. The viral burden also started dropping down in the nasal regions at 4 dpi, causing less penetrable to the lungs in the case of Omicron infection at 4 dpi which further explains its lower replication efficiency as opposed to the Delta variant. These data were consistent with earlier observations studied on hamsters (21). The earlier *in vitro* comparative studies on growth kinetics of the Delta and Omicron variants in Calu3 cells, a lung epithelial cell line, have shown that the Omicron has a poor replication rate which correlates with our findings of low lung viral copy number observed in Omicron infected hamsters (22). We observed severe and diffused lung histopathological lesions with higher inflammatory cytokine levels in Delta-infected groups when compared to Hongkong and Omicron-infected groups. An earlier report on lung pathology during Omicron-infection in the hamster model showed that lung disease is milder in the Omicron group and highest in the Delta groups when compared to ancestral SARS-CoV-2 (23, 24). Also, contrary to our findings, a study reported moderate to severe changes in the lungs of Omicron-infected hamsters which were almost comparable to their Delta-infected group (25). Coronaviruses are known causative agents of both respiratory and gastrointestinal tract infections in a wide range of mammals and birds (26). Also, SARS-CoV-2 cell tropism was shown in multiple organs of human post-mortem samples including lungs, trachea, small intestines, and other tissues (11). SARS-CoV-2 has been shown earlier to infect and replicate in both bat and human intestinal organoids, leading to viral replication within these cells (22). Besides that, *in vitro* studies have shown the higher replicative ability of the Delta strain in human colon epithelial cell lines such as Caco2 than Omicron or other strains (27).

ACE2 is known to be an essential receptor for virus entry into the host cells and its expression level differs among organs and tissues which might determine the symptoms and outcome of COVID-19. ACE2 expression levels are highest in the

small intestine which suggests that the gastrointestinal tract could be a potential site of viral replication and transmission (28). Along with ACE2, SARS-CoV-2 entry was shown to be dependent on transmembrane serine protease 2 (TMPRSS2), a host protease, which cleaves the viral spike protein once it binds to the ACE2 receptor. The TMPRSS2 expression is also spread across the GI tract. Indeed, the co-expression of ACE2 and TMPRSS2 is highest in human nasal and intestinal epithelial cells with relatively lesser levels in lung and esophageal cells (29). In alignment with this data, the viral RNA was detected in hamsters at a high copy number in the esophagus, stomach, and small intestine, indicating that the virus is directly interacting by binding to the cells of the GI tract. The Delta variant being more replicative and further elevating the levels of inflammatory markers such as IFN-□, TNF-α, and IL-6 shows permissiveness of the intestinal cells and higher pathogenicity of the specific SARS-CoV-2 strain.

The reduced viral load in the large intestine and fecal samples could be mostly specific to the hamster infection model. While GI symptoms are predominantly seen in the severe form of COVID-19 patients (30), hamsters won't show such severe symptoms of SARS-CoV-2 infection, which could be a possible reason for us not being able to detect viral RNA in hamster fecal samples collected on 4 dpi. Additionally, earlier reports showed better ACE2 expression levels in the esophagus, duodenum, and ileum regions of Syrian hamsters with no expression in the large intestine (31). This correlates with our data, as the large intestine had less viral burden which might have reduced the fecal transmission in hamsters. Nevertheless, based on the meta-analysis data, the rate of GI infection and detection of viral RNA in stool samples is under 53 % (32). Also, though the viral RNA gets detected in the respiratory tract at earlier time points, it takes additional 4-5 days to show up in the human stool samples (33).

The villous blunting and increased epithelial regeneration in the duodenal samples of COVID-19 patients have been reported which is consistent with our study where regenerative changes were observed in the duodenum, especially among the Delta-infected hamsters (34). Even though no apparent inflammation was present, viral nucleocapsid protein could be detected in the duodenal epithelial cells of animals infected with the Delta strain (35). This resembles the detection of SARS-CoV-2 protein in intestinal samples of human covid patients without apparent architectural

disruption (33). Overall, the experimental data suggest that the Omicron strain is less pathogenic and less transmissible when compared to the other two strains. Even though, Delta and Hongkong strains showed similar viral burdens in many organs, the Delta strain distinguished itself by causing more severe clinical signs, viral burden, cellular inflammation, and pathology, especially in the small intestine of hamsters. The Syrian hamster was also shown here to be permissive to SARS-CoV-2 in the gastrointestinal tract, where the Delta strain exhibited higher tissue tropism.

The limitations of the study are that, firstly, the gap between the inoculum dose is relatively lesser which could be a reason for not observing a significant difference in the parameters studied between the two doses of inoculums used. Secondly, the use of more animals per group could improve the higher correlation among the different data generated. Nevertheless, this study warrants further exploration of host factors required for GI tropism and associated disease by SARS-CoV-2 and other human coronaviruses.

Acknowledgments

This work is supported by DBT-BIRAC (BT/CS0007/CS/02/20) and DBT-Wellcome Trust India Alliance (IA/I/18/1/503613) grant to STacknowledge infrastructure and research support to IISc from the Crypto Relief Fund, L & T Trust, DST-FIST program, Institute of Eminence Fund, Ministry of Education, and DBT-IISc partnership program (Phase II). OK, SK and RS acknowledge support from the MHRD-IISc fellowship and Prime Minister's Research Fellowship (PMRF) and FICCI-PMRF respectively.

Conflict of Interest

Authors have no conflicts of interest to declare.

References

1. Gorbalenya AE, Baker SC, Baric RS, de Groot RJ, Drosten C, Gulyaeva AA, et al. The species Severe acute respiratory syndrome-related coronavirus: classifying 2019-nCoV and naming it SARS-CoV-2. 2020;5(4):536-44.
2. V'kovski P, Kratzel A, Steiner S, Stalder H, Thiel V. Coronavirus biology and replication: implications for SARS-CoV-2. Nature Reviews Microbiology. 2021;19(3):155-70.
3. Letko M, Marzi A, Munster V. Functional assessment of cell entry and receptor usage for SARS-CoV-2 and other lineage B betacoronaviruses. Nature microbiology. 2020;5(4):562-9.

472 4. Koch J, Uckeley ZM, Doldan P, Stanifer M, Boulant S, Lozach PY. TMPRSS2 expression dictates
473 the entry route used by SARS-CoV-2 to infect host cells. Embo j. 2021;40(16):e107821.
474 5. Hui DS, Azhar EI, Madani TA, Ntoumi F, Kock R, Dar O, et al. The continuing 2019-nCoV
475 epidemic threat of novel coronaviruses to global health—The latest 2019 novel coronavirus outbreak
476 in Wuhan, China. 2020;91:264-6.
477 6. Andersen KG, Rambaut A, Lipkin WI, Holmes EC, Garry RF. The proximal origin of SARS-CoV-2.
478 Nat Med. 2020;26(4):450-2.
479 7. Phan T. Genetic diversity and evolution of SARS-CoV-2. Infection, genetics and evolution :
480 journal of molecular epidemiology and evolutionary genetics in infectious diseases. 2020;81:104260.
481 8. Carabelli AM, Peacock TP, Thorne LG, Harvey WT, Hughes J, de Silva TI, et al. SARS-CoV-2
482 variant biology: immune escape, transmission and fitness. Nature Reviews Microbiology.
483 2023;21(3):162-77.
484 9. Tegally H, Moir M, Everatt J, Giovanetti M, Scheepers C, Wilkinson E, et al. Emergence of
485 SARS-CoV-2 Omicron lineages BA.4 and BA.5 in South Africa. Nature Medicine. 2022;28(9):1785-90.
486 10. Gupta A, Madhavan MV, Sehgal K, Nair N, Mahajan S, Sehrawat TS, et al. Extrapulmonary
487 manifestations of COVID-19. Nature Medicine. 2020;26(7):1017-32.
488 11. Liu J, Li Y, Liu Q, Yao Q, Wang X, Zhang H, et al. SARS-CoV-2 cell tropism and multiorgan
489 infection. Cell Discovery. 2021;7(1):17.
490 12. Carrau L, Frere JJ, Golynker I, Fajardo A, Rivera CF, Horiuchi S, et al. Delayed engagement of
491 host defenses enables SARS-CoV-2 viremia and productive infection of distal organs in the hamster
492 model of COVID-19. Science signaling. 2023;16(789):eadg5470.
493 13. Rosenke K, Meade-White K, Letko M, Clancy C, Hansen F, Liu Y, et al. Defining the Syrian
494 hamster as a highly susceptible preclinical model for SARS-CoV-2 infection. Emerging microbes &
495 infections. 2020;9(1):2673-84.
496 14. Imai M, Iwatsuki-Horimoto K, Hatta M, Loeber S, Halfmann PJ, Nakajima N, et al. Syrian
497 hamsters as a small animal model for SARS-CoV-2 infection and countermeasure development.
498 Proceedings of the National Academy of Sciences of the United States of America.
499 2020;117(28):16587-95.
500 15. Boudewijns R, Thibaut HJ, Kaptein SJF, Li R, Vergote V, Seldeslachts L, et al. STAT2 signaling
501 restricts viral dissemination but drives severe pneumonia in SARS-CoV-2 infected hamsters. Nat
502 Commun. 2020;11(1):5838.
503 16. Case JB, Bailey AL, Kim AS, Chen RE, Diamond MS. Growth, detection, quantification, and
504 inactivation of SARS-CoV-2. Virology. 2020;548:39-48.
505 17. Tostanoski LH, Wegmann F, Martinot AJ, Loos C, McMahan K, Mercado NB, et al. Ad26
506 vaccine protects against SARS-CoV-2 severe clinical disease in hamsters. Nature Medicine.
507 2020;26(11):1694-700.
508 18. European Centre for Disease Prevention and Control. Threat assessment brief: emergence of
509 SARS-CoV-2 B.1.617 variants in India and situation in the EU/EEA

510 2021.
511 19. Viana R, Moyo S, Amoako DG, Tegally H, Scheepers C, Althaus CL, et al. Rapid epidemic
512 expansion of the SARS-CoV-2 Omicron variant in southern Africa. 2022;603(7902):679-86.
513 20. Chakraborty C, Bhattacharya M, Sharma AR, Dhama K, Lee S-S. The rapid emergence of
514 multiple sublineages of Omicron (B.1.1.529) variant: Dynamic profiling via molecular phylogenetics
515 and mutational landscape studies. Journal of Infection and Public Health. 2022;15(11):1234-58.
516 21. Toomer G, Burns W, Garcia L, Henry G, Biancofiori A, George A, et al. Characterization of
517 Three Variants of SARS-CoV-2 In Vivo Shows Host-Dependent Pathogenicity in Hamsters, While Not in
518 K18-hACE2 Mice. Viruses. 2022;14(11).
519 22. Zhou J, Li C, Liu X, Chiu MC, Zhao X, Wang D, et al. Infection of bat and human intestinal
520 organoids by SARS-CoV-2. Nat Med. 2020;26(7):1077-83.
521 23. Yuan S, Ye ZW, Liang R, Tang K, Zhang AJ, Lu G, et al. Pathogenicity, transmissibility, and
522 fitness of SARS-CoV-2 Omicron in Syrian hamsters. Science. 2022;377(6604):428-33.

523 24. Suzuki R, Yamasoba D, Kimura I, Wang L, Kishimoto M, Ito J, et al. Attenuated fusogenicity
524 and pathogenicity of SARS-CoV-2 Omicron variant. Nature. 2022;603(7902):700-5.
525 25. Mohandas S, Yadav PD, Sapkal G, Shete AM, Deshpande G, Nyayanit DA, et al. Pathogenicity
526 of SARS-CoV-2 Omicron (R346K) variant in Syrian hamsters and its cross-neutralization with different
527 variants of concern. EBioMedicine. 2022;79:103997.
528 26. Chan JF, To KK, Tse H, Jin DY, Yuen KY. Interspecies transmission and emergence of novel
529 viruses: lessons from bats and birds. Trends in microbiology. 2013;21(10):544-55.
530 27. Mautner L, Hoyos M, Dangel A, Berger C, Ehrhardt A, Baiker A. Replication kinetics and
531 infectivity of SARS-CoV-2 variants of concern in common cell culture models. Virol J. 2022;19(1):76.
532 28. Zhang H, Li HB, Lyu JR, Lei XM, Li W, Wu G, et al. Specific ACE2 expression in small intestinal
533 enterocytes may cause gastrointestinal symptoms and injury after 2019-nCoV infection. International
534 journal of infectious diseases : IJID : official publication of the International Society for Infectious
535 Diseases. 2020;96:19-24.
536 29. Sungnak W, Huang N, Bécavin C, Berg M, Queen R, Litvinukova M, et al. SARS-CoV-2 entry
537 factors are highly expressed in nasal epithelial cells together with innate immune genes. Nat Med.
538 2020;26(5):681-7.
539 30. Arjmand B, Ghorbani F, Koushki M, Rezai-Tavirani M. Gastrointestinal symptoms in patients
540 with mild and severe COVID-19: a scoping review and meta-analysis. Gastroenterology and
541 hepatology from bed to bench. 2020;13(4):321-30.
542 31. Suresh V, Parida D, Minz AP, Sethi M, Sahoo BS, Senapati S. Tissue Distribution of ACE2
543 Protein in Syrian Golden Hamster (Mesocricetus auratus) and Its Possible Implications in SARS-CoV-2
544 Related Studies. Frontiers in pharmacology. 2020;11:579330.
545 32. Tian Y, Rong L, Nian W, He Y. Review article: gastrointestinal features in COVID-19 and the
546 possibility of faecal transmission. Alimentary pharmacology & therapeutics. 2020;51(9):843-51.
547 33. Xiao F, Tang M, Zheng X, Liu Y, Li X, Shan H. Evidence for Gastrointestinal Infection of SARS-
548 CoV-2. Gastroenterology. 2020;158(6):1831-3.e3.
549 34. Lehmann M, Allers K, Heldt C, Meinhardt J, Schmidt F, Rodriguez-Sillke Y, et al. Human small
550 intestinal infection by SARS-CoV-2 is characterized by a mucosal infiltration with activated CD8(+) T
551 cells. Mucosal immunology. 2021;14(6):1381-92.
552 35. Sia SF, Yan LM, Chin AWH, Fung K, Choy KT, Wong AYL, et al. Pathogenesis and transmission
553 of SARS-CoV-2 in golden hamsters. Nature. 2020;583(7818):834-8.

554

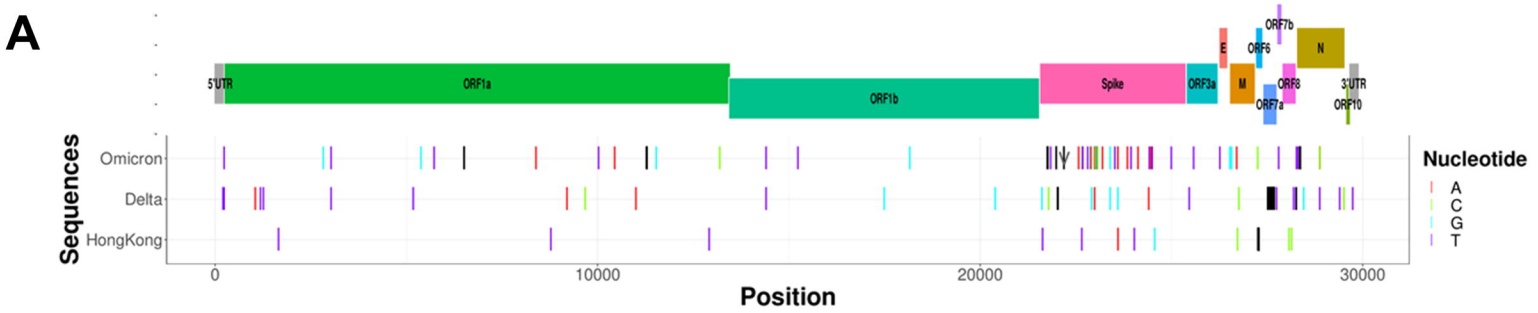
A
5'UTR
ORF1a
ORF1b
Spike
ORF3a
E
M
ORF6
ORF7b
ORF7a
ORF8
N
3'UTR
ORF10
Sequences
Omicron
Delta
HongKong
Nucleotide
A
C
G
T
0
10000
20000
30000
Position

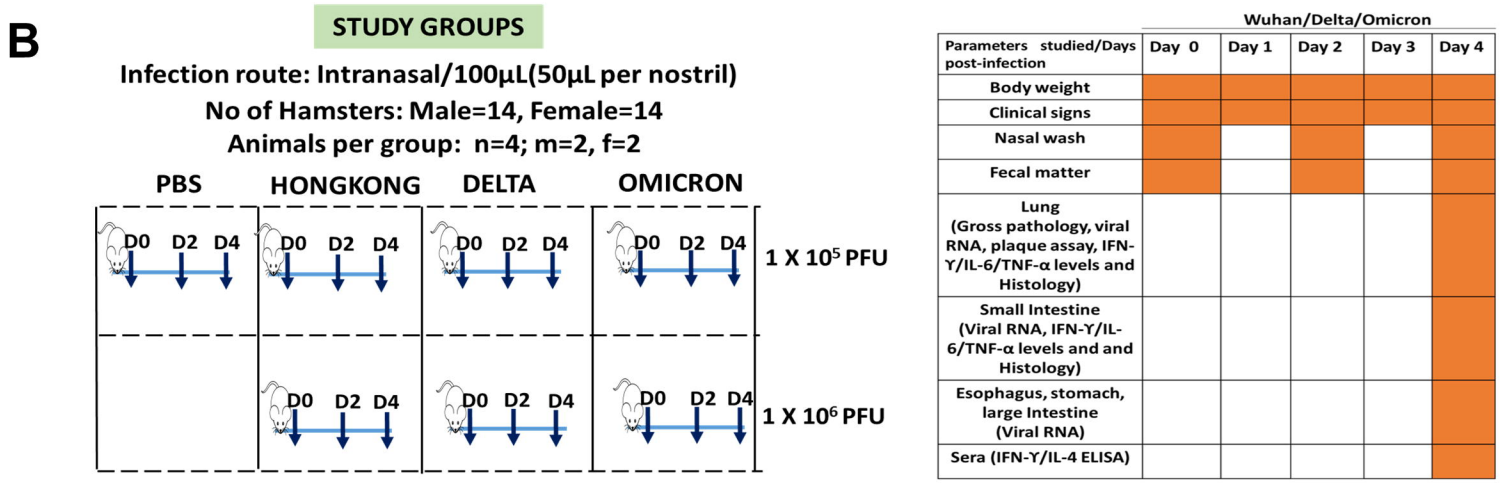
B
STUDY GROUPS
Infection route: Intranasal/100µL(50µL per nostril)
No of Hamsters: Male=14, Female=14
Animals per group: n=4; m=2, f=2
PBS
HONGKONG
DELTA
OMICRON
D0 D2 D4
1 X 10⁵ PFU
1 X 10⁶ PFU
Wuhan/Delta/Omicron
Parameters studied/Days post-infection
Day 0
Day 1
Day 2
Day 3
Day 4
Body weight
Clinical signs
Nasal wash
Fecal matter
Lung (Gross pathology, viral RNA, plaque assay, IFN-γ/IL-6/TNF-α levels and Histology)
Small Intestine (Viral RNA, IFN-γ/IL-6/TNF-α levels and and Histology)
Esophagus, stomach, large Intestine (Viral RNA)
Sera (IFN-γ/IL-4 ELISA)

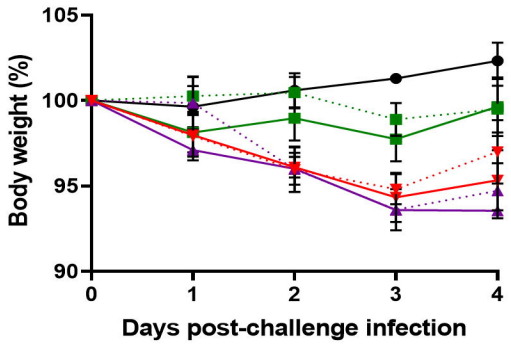
C
Body weight (%)
105
100
95
90
0
1
2
3
4
Days post-challenge infection

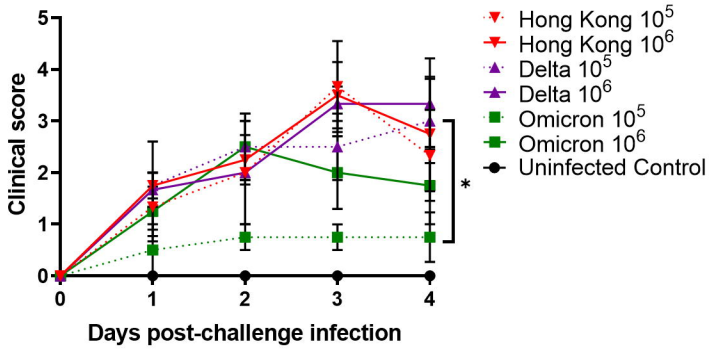
D
Clinical score
5
4
3
2
1
0
*
Hong Kong 10⁵
Hong Kong 10⁶
Delta 10⁵
Delta 10⁶
Omicron 10⁵
Omicron 10⁶
Uninfected Control
Days post-challenge infection

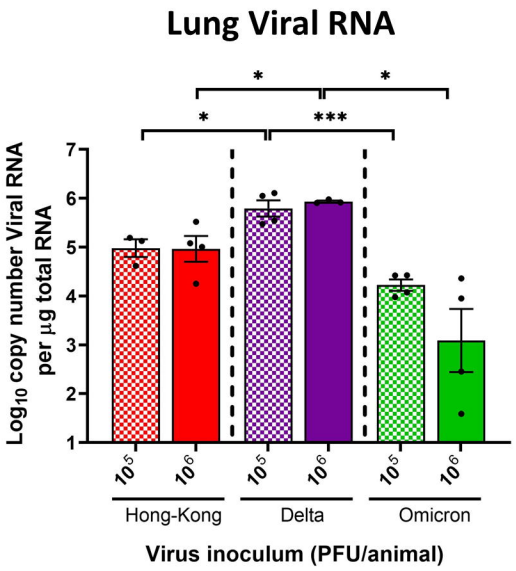
Lung Viral RNA
E
Log10 copy number Viral RNA per µg total RNA
7
6
5
4
3
2
1
*
*
*
***
10⁵
10⁶
Hong-Kong
Delta
Omicron
Virus inoculum (PFU/animal)

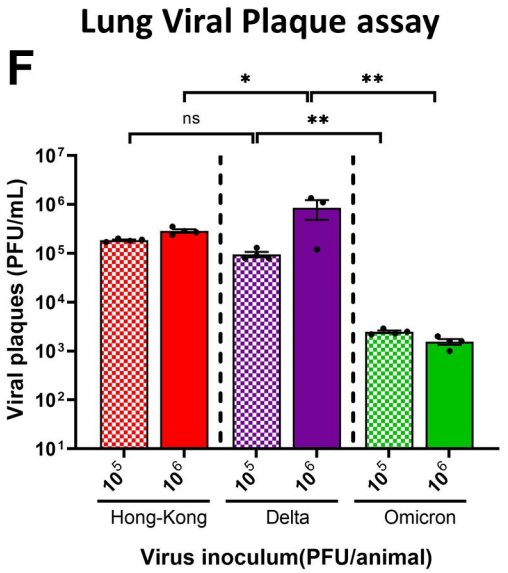
Lung Viral Plaque assay
F
Viral plaques (PFU/mL)
10⁷
10⁶
10⁵
10⁴
10³
10²
10¹
*
**
ns
**
10⁵
10⁶
Hong-Kong
Delta
Omicron
Virus inoculum(PFU/animal)

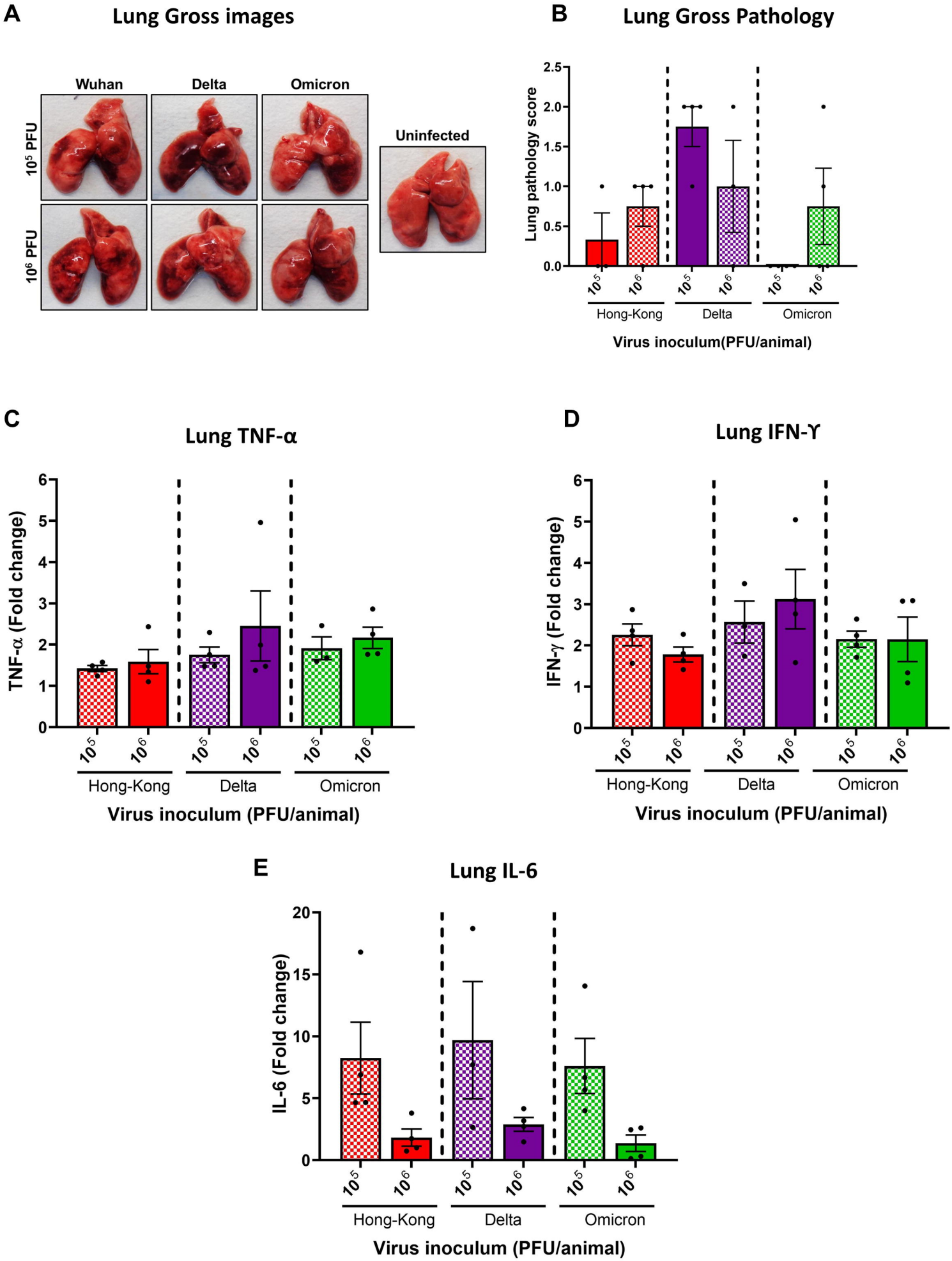
A
Lung Gross images
Wuhan
Delta
Omicron
Uninfected
10^5 PFU
10^6 PFU
B
Lung Gross Pathology
Lung pathology score
2.5
2.0
1.5
1.0
0.5
0.0
10^5
10^6
Hong-Kong
Delta
Omicron
Virus inoculum(PFU/animal)
C
Lung TNF-α
TNF-α (Fold change)
6
5
4
3
2
1
0
10^5
10^6
Hong-Kong
Delta
Omicron
Virus inoculum (PFU/animal)
D
Lung IFN-ϒ
IFN-γ (Fold change)
6
5
4
3
2
1
0
10^5
10^6
Hong-Kong
Delta
Omicron
Virus inoculum (PFU/animal)
E
Lung IL-6
IL-6 (Fold change)
20
15
10
5
0
10^5
10^6
Hong-Kong
Delta
Omicron
Virus inoculum (PFU/animal)

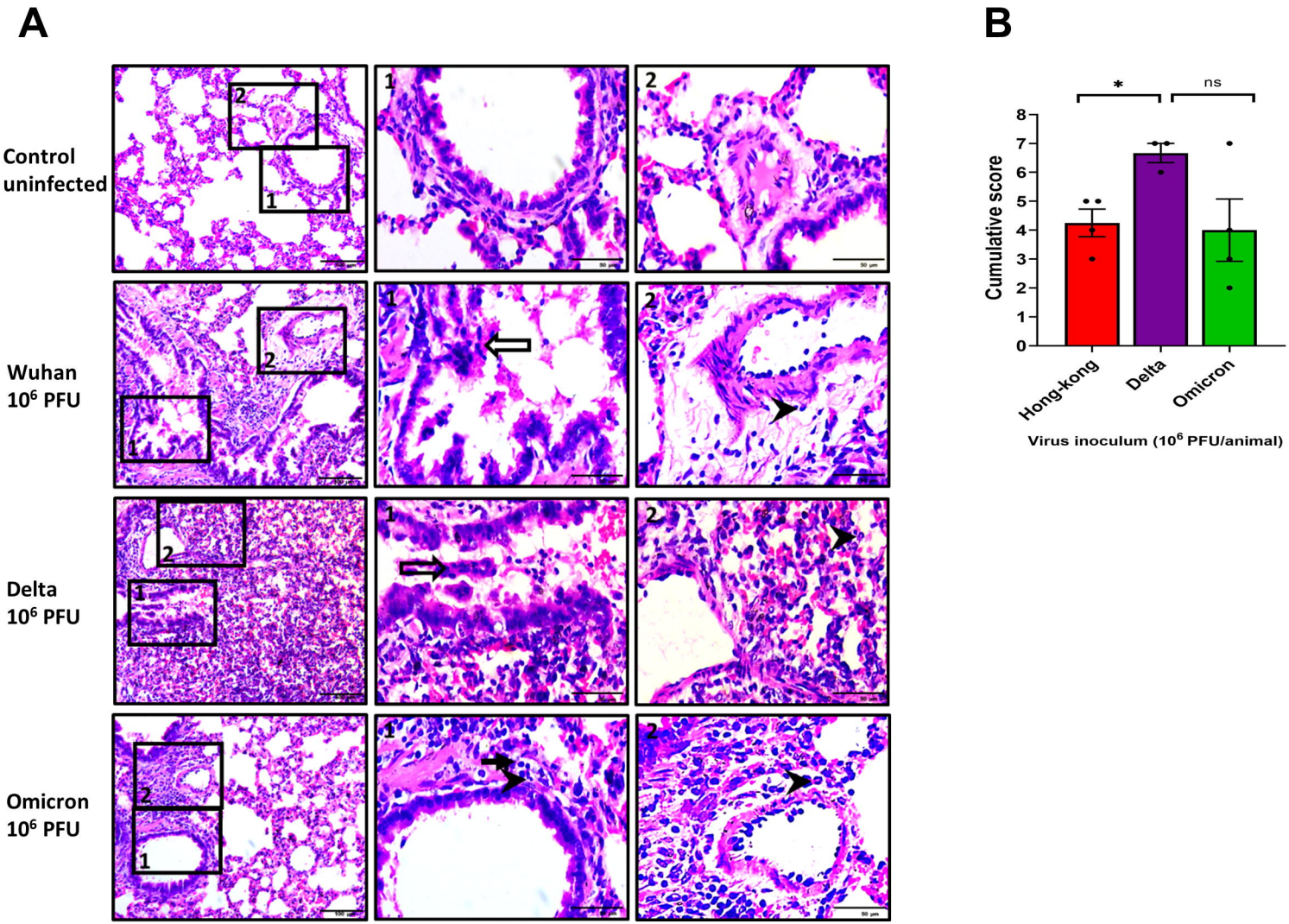
A
Control uninfected
Wuhan 10^6 PFU
Delta 10^6 PFU
Omicron 10^6 PFU
B
*
ns
Cumulative score
0
1
2
3
4
5
6
7
8
Hong-kong
Delta
Omicron
Virus inoculum (10^6 PFU/animal)

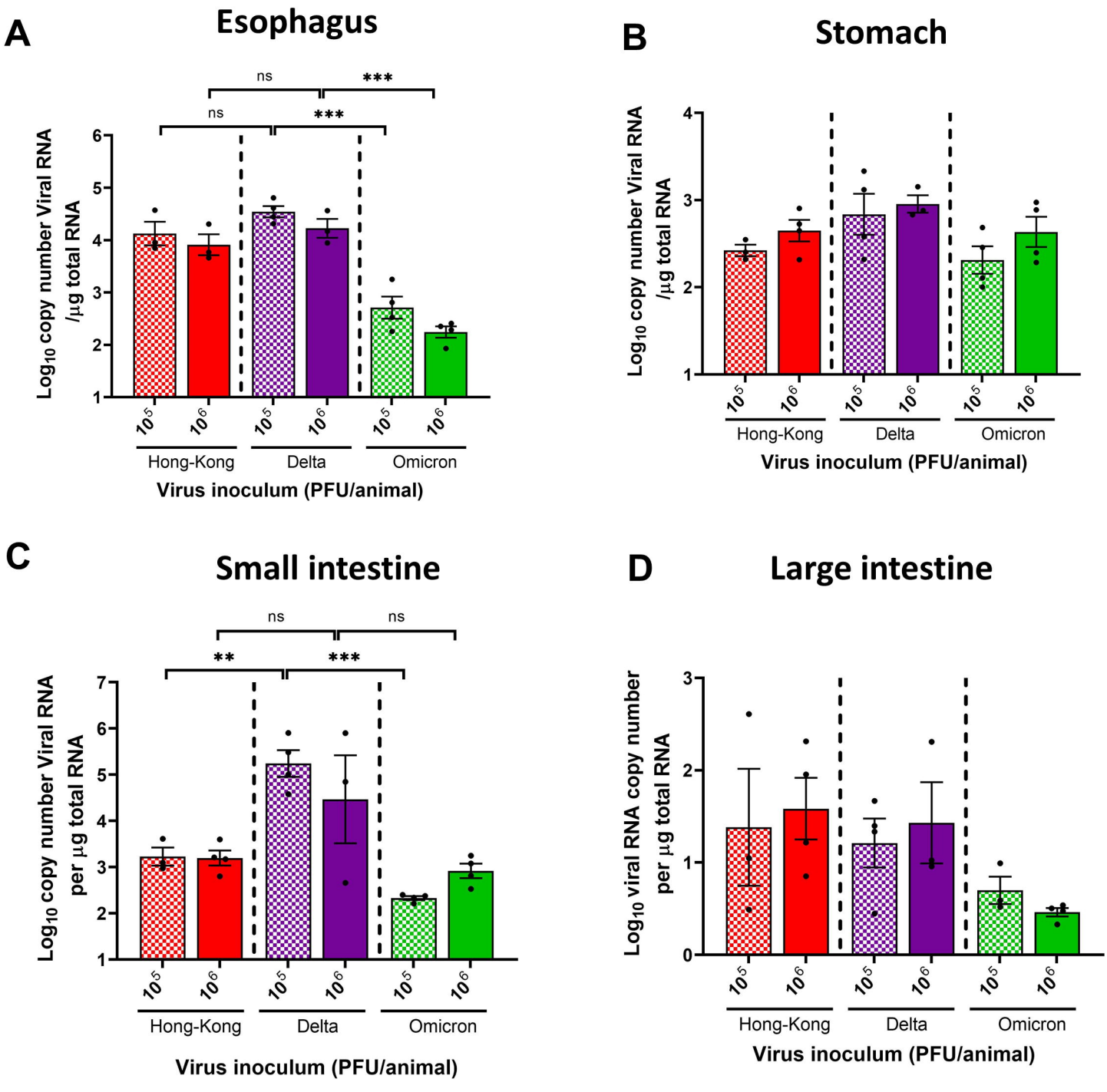
A
Esophagus
ns
***
ns
***
Log10 copy number Viral RNA /µg total RNA
6
5
4
3
2
1
10^5
10^6
10^5
10^6
10^5
10^6
Hong-Kong
Delta
Omicron
Virus inoculum (PFU/animal)
B
Stomach
Log10 copy number Viral RNA /µg total RNA
4
3
2
1
10^5
10^6
10^5
10^6
10^5
10^6
Hong-Kong
Delta
Omicron
Virus inoculum (PFU/animal)
C
Small intestine
ns
ns
**
***
Log10 copy number Viral RNA per µg total RNA
7
6
5
4
3
2
1
10^5
10^6
10^5
10^6
10^5
10^6
Hong-Kong
Delta
Omicron
Virus inoculum (PFU/animal)
D
Large intestine
Log10 viral RNA copy number per µg total RNA
3
2
1
0
10^5
10^6
10^5
10^6
10^5
10^6
Hong-Kong
Delta
Omicron
Virus inoculum (PFU/animal)

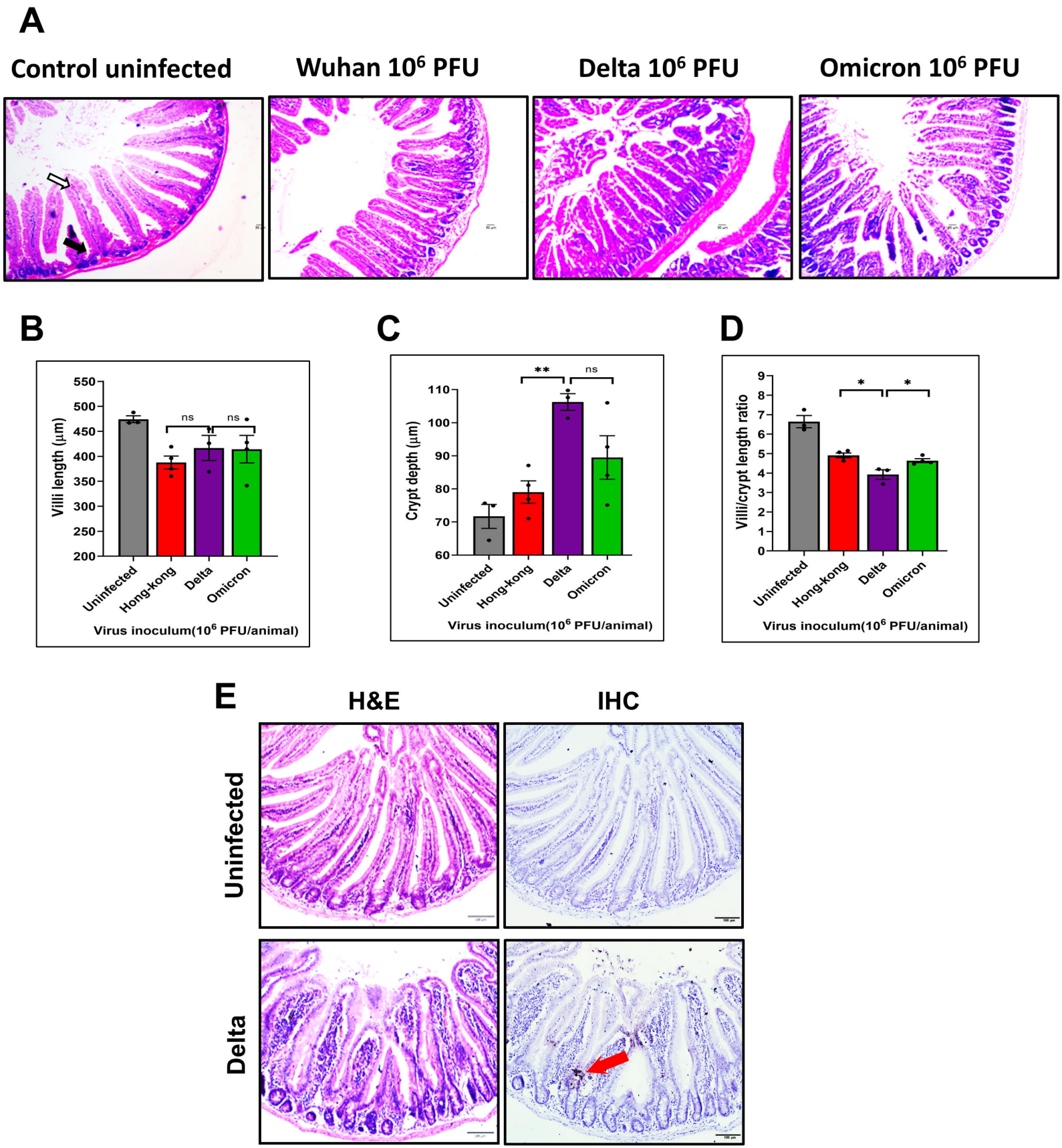
A
Control uninfected
Wuhan 10^6 PFU
Delta 10^6 PFU
Omicron 10^6 PFU
B
Villi length (μm)
550
500
450
400
350
300
250
200
ns
ns
Uninfected
Hong-kong
Delta
Omicron
Virus inoculum(10^6 PFU/animal)
C
Crypt depth (μm)
110
100
90
80
70
60
**
ns
Uninfected
Hong-kong
Delta
Omicron
Virus inoculum(10^6 PFU/animal)
D
Villi/crypt length ratio
9
8
7
6
5
4
3
2
1
0
*
*
Uninfected
Hong-kong
Delta
Omicron
Virus inoculum(10^6 PFU/animal)
E
H&E
IHC
Uninfected
Delta